Direct measurement of the effective charge in nonpolar suspensions by optical tracking of single particles

G. Seth Roberts and Tiffany A. Wood
School of Chemistry, University of Bristol, Bristol BS8 1TS, United Kingdom

William J. Frith
Unilever Research Colworth, Colworth House, Sharnbrook, Bedford MK44 1LQ, United Kingdom

Paul Bartlett[a)]
School of Chemistry, University of Bristol, Bristol BS8 1TS, United Kingdom

(Received 19 January 2007; accepted 3 April 2007; published online 16 May 2007)

The authors develop an ultrasensitive method for the measurement of the charge carried by a colloidal particle in a nonpolar suspension. The technique uses the phenomenon of the resonance of a particle held in an optical tweezer trap and driven by a sinusoidal electric field. The trapped particle forms a strongly damped harmonic oscillator whose fluctuations are a function of γ, the ratio of the root-mean-square average of the electric and thermal forces on the particle. At low applied fields ($\gamma \ll 1$) the particle is confined to the optical axis, while at high fields ($\gamma \gg 1$) the probability distribution of the particle is double peaked. The periodically modulated thermal fluctuations are measured with nanometer sensitivity using an interferometric position detector. Charges, as low as a few elementary charges, can be measured with an uncertainty of about $0.25e$. This is significantly better than previous techniques and opens up new possibilities for the study of nonpolar suspensions. © *2007 American Institute of Physics*. [DOI: 10.1063/1.2734968]

I. INTRODUCTION

Although charge is often thought to play no role in nonpolar media, there is ample,[1–3] if sometimes contradictory,[4] evidence of surface charging in nonpolar colloidal suspensions. Much of the reason for this uncertainty is the extremely low level of charge in nonpolar environments. While a particle of radius $a \sim 500$ nm might carry a surface charge eZ of the order of 10^3 electrons in an aqueous dispersion ($\epsilon_r \sim 80$), the charge in a nonpolar solvent will be some two or three orders of magnitude smaller. Although small in absolute terms, this charge still produces surprisingly strong effects in low dielectric environments. For instance, using Coulomb's law, the contact value of the interaction potential (in units of k_BT) between two colloidal spheres with radius a and charge eZ in a solvent of dielectric ratio ϵ_r is simply

$$\frac{U_0}{k_BT} = \frac{1}{k_BT} \cdot \frac{Z^2e^2}{8\pi\epsilon_0\epsilon_r a} = \left(\frac{\lambda_B}{2a}\right)Z^2, \tag{1}$$

where we have introduced the Bjerrum length $\lambda_B = e^2/4\pi\epsilon_0\epsilon_r k_BT$ as a characteristic length scale of electrostatic interactions. For dodecane, λ_B is 28.0 nm so the repulsive interactions between 500 nm particles, carrying a typical charge of $10e$, is $\approx 3k_BT$—big enough to have a dramatic effect on the structure of a colloidal suspension.

The most direct route to monitor the extent of particle charging is to measure the uniform drift velocity u_D in the presence of a weak electric field E. For a spherical particle, $u_D = \mu E$, where μ is the electrophoretic mobility. The electrophoretic mobility of an isolated particle in a solvent of viscosity η is related to the electrostatic potential ζ at the hydrodynamic slipping plane of the particle by the linear relationship

$$\mu = f\frac{\epsilon_0\epsilon_r\zeta}{\eta}, \tag{2}$$

where ζ is small ($e\zeta \lesssim k_BT$).[5] The prefactor f depends on the dimensionless ratio of the particle radius a to the Debye screening length $\kappa^{-1} = 1/\sqrt{4\pi\rho_0\lambda_B}$, where ρ_0 is the number density of singly charged ions in solution. The Smoluchowski equation ($f=1$) is valid in the limiting case where $\kappa a \to \infty$, while the Hückel equation ($f=2/3$) is valid in the case of a very diffuse ionic atmosphere where $\kappa a \to 0$. For arbitrary κa, Henry[5] derived an expression for f, accurate for small ζ, which took into account retardation effects and interpolates between the limiting cases of very thin and very thick electrical double layers. For high ζ potentials ($e\zeta \gg k_BT$), where the deformation of the electrical double layer becomes significant, the mobility is no longer simply proportional to ζ and the full numerical solutions of O'Brien and White[6] must be used for isolated spheres (standard electrokinetic model). At finite concentrations more advanced theories need to be used.[7] In nonpolar suspensions, where typically zeta potentials are small and ion concentrations are low ($\kappa a \ll 1$), the Hückel limiting case is normally valid. Equation (2) with $f=2/3$ can be rewritten in terms of the electrokinetic charge Ze on the particle,

$$\mu = Ze/(6\pi\eta a), \tag{3}$$

where $Ze = 4\pi\epsilon_0\epsilon_r a(1+\kappa a)\zeta$. The low charges found in nonpolar media therefore translate to electrophoretic mobilities

[a)]Electronic mail: p.bartlett@bristol.ac.uk

some two or three orders of magnitude or so less than in water, at the same electric field. A rapid and reproducible measurement of these low mobilities presents a major challenge to conventional electrokinetic techniques.[1]

Motivated by the growing acknowledgment of the importance of charge in nonpolar suspensions[8] and its technological significance,[9] several novel methods have been developed to determine particle mobility in nonpolar suspensions. Schätzel and co-workers[10] pioneered an innovative amplitude-weighted phase analysis signal processing scheme for the analysis of classical laser Doppler electrophoresis data. The technique, phase analysis light scattering (PALS), is significantly more sensitive than conventional laser Doppler electrophoresis. In practice, however, a collective particle motion induced by thermal convection or sedimentation restricts the achievable sensitivity of commercial PALS instruments to $\sim 10^{-10}$ m^2 s^{-1} V^{-1}, which corresponds to colloid charges of $\sim 10e$ on a particle of radius $a=500$ nm. Video microscopy has been used by several authors. Perez and Lemaire[11] used a vibrating piezoelectric stage to null the oscillatory microscopic motion produced by an applied alternating field, while Strubbe *et al.*[12] measured the diffusion constant and electrophoretic mobility of individual particles in a nonpolar suspension. Despite these developments, there is still no technique which can provide a fast and accurate measurement of the extremely small levels of particle charge found in nonpolar suspensions. As a result, the microscopic charging mechanisms in nonaqueous media have remained largely problematic.[4] Improvements in quantitative characterization are an essential first step to developing a more detailed understanding of the role of charge in nonpolar suspensions.

In this paper, we present direct measurements of the magnitude and frequency dependence of the effective charge on single isolated colloidal particles in a nonpolar solvent. Radiation pressure from a laser beam focused to a near-diffraction-limited spot (an "optical tweezer") is used to trap individual colloidal particles. The laser and trapped particle constitute a harmonic oscillator with a stiffness which is proportional to the laser power. The hindered diffusion of the trapped colloid is modified by an oscillatory electric field. The charge is directly obtained in the time domain by autocorrelation of the change in the Brownian motion of the particle produced by the application of an alternating electric field. We demonstrate that by using a low intensity laser trap combined with an interferometric position detection system, we can measure accurately a mean particle charge of $-2.9e$ which, for the typical field strengths used, corresponds to an electric force of about 40 fN. We estimate that the sensitivity of our technique is about an order of magnitude smaller than this limit. The method is a significant improvement on existing techniques for the characterization of nonpolar suspensions. It provides rapid, accurate, and highly sensitive information on the level of charge on isolated colloidal particles in nonpolar suspensions. Related but less sensitive experiments have been described on highly charged aqueous colloids by Garbow *et al.*,[13] where the authors used a weakly focused laser beam. This had the effect of pushing particles along the optical axis, rather than stably confining them, as in our approach. A similar technique to the one presented here came to our knowledge after the preparation of this paper. It has been previously used by Galneder *et al.*[14] to monitor the enzyme-catalyzed hydrolysis of a charged phospholipid bilayer deposited on an aqueous silica bead with a sensitivity of ~ 10 mV of zeta potential. These authors focused on the biophysical applications, while the present paper presents a full account of the measuring theory and a thorough characterization of the technique, its performance, and accuracy. In addition, interesting applications to nonpolar suspensions are given, and the usefulness and limits of this approach in addressing some important questions concerning these systems are discussed in detail.

This paper is organized as follows: After a description of the apparatus and measurement procedures, we give a short introduction to the theory of a driven overdamped harmonic oscillator before results obtained on a variety of different nonpolar suspensions are presented and discussed in the final section.

II. MATERIALS AND METHODS

A. Materials

We use a model nonaqueous colloidal system of sterically stabilized poly(methyl methacrylate) (PMMA) spheres of radius $a=610\pm30$ nm suspended in dodecane. The particles were synthesized by dispersion polymerization, following the procedures detailed by Antl *et al.*,[15] and stabilized by a comb copolymer of poly(12-hydroxy stearic acid) (PHSA) and PMMA. Electron microscopy revealed that the particles were highly uniform in size with a radius polydispersity (root-mean-square variation/mean radius) of $\sigma=0.046\pm0.01$. Dodecane was dried with activated molecular sieves (Acros, size 4A) and stored under dry nitrogen. Sodium bis(2-ethylhexyl) sulfosuccinate (NaAOT, Fluka BioChemika Ultra 99%) was purified by dissolution in methanol and tumbled with activated charcoal. Zirconyl 2-ethyl hexanoate $[Zr(Oct)_2]$ was purchased from Alfa Aesar (Heysham, UK) and used as received. Debye lengths were estimated from conductivity measurements and the dimensions of the inverse micelles as determined by small-angle neutron scattering.

B. Optical tweezers

Figure 1 shows a schematic of our optical tweezer system. A fiber-coupled laser beam with wavelength $\lambda=1064$ nm (ytterbium fiber laser, IPG Photonics, Germany) was focused to a diffraction-limited beam waist by a microscope objective (Plan-Neofluar, ×100, numerical aperture (NA) 1.3, Zeiss) mounted in an inverted microscope (Axiovert S100, Zeiss). The laser power (~ 10 mW) was varied using a $\lambda/2$ wave plate and a polarizing beam-splitter cube placed in the beam path. The fluctuations in the position of the trapped particle, with respect to the center of the trap, were measured with a quadrant photodetector (model QD50-4X, Centronics, UK) using back-plane optical interferometry.[16] The particle positions were acquired by a LABVIEW program (National Instruments, Austin, Texas, USA) and digitized using a high-speed data acquisition card

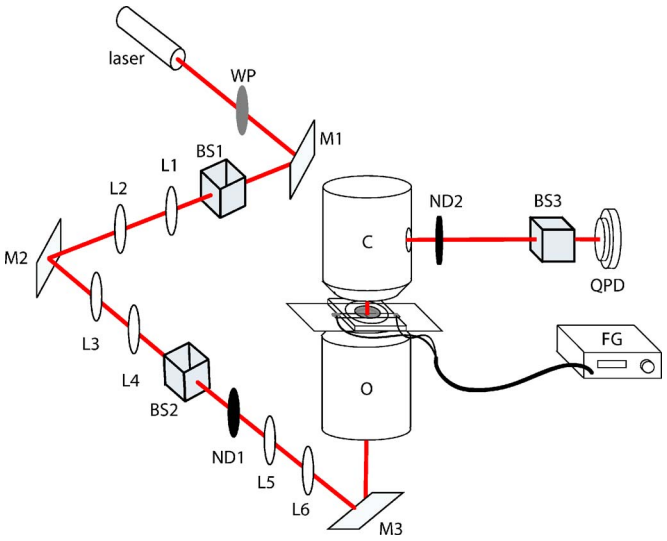

FIG. 1. (Color online) Simplified experimental setup of optical microelectrophoresis apparatus. WP, λ/2 wave plate; M, gimbal mirror; BS, beam-splitting cube; L, lens; ND, neutral density filter; O, oil-immersion objective; C, high NA condenser; QPD, quadrant photodetector; FG, function generator.

(National Instruments model PCI-MI0-16E-1) at 10 kHz. For the current experiments, the number of particle positions collected in each time trace was set at 2^{18}, so that the duration of each measurement was ≈26 s. Positions measured in voltages were converted into displacements in nanometers by recording the time-dependent mean-square voltage $\langle \Delta V^2(\tau) \rangle$ of five particles from the same batch of particles, immediately before each set of electrophoresis measurements. Assuming that the voltage recorded is proportional to the displacement, $\langle \Delta V^2(\tau) \rangle$ was fitted to the theoretical expression for the mean-square displacement $\langle \Delta x^2(\tau) \rangle$ of a Brownian sphere in a harmonic potential to yield the detector calibration and trap stiffness k_H. The laboratory temperature was stabilized at 22±1 °C. At this temperature the viscosity of dodecane is 1.378×10^{-3} Pa s and the dielectric constant is 2.002.

C. Single particle optical microelectrophoresis (SPOM)

The microelectrophoresis cell was constructed from two platinum foil electrodes, 127 μm high and 2 mm wide, mounted in a cylindrical glass sample chamber, 1.13 mm high. The sample volume was ~90 μl. The cell was constructed in three stages. First, two platinum foil electrodes were carefully positioned parallel to each other on a 5.0 ×2.5 cm^2 rectangular glass coverslip (170 μm thick), covered with a thick layer of a UV-activated glue (Loctite 350), using a low-magnification stereo microscope. The electrodes were securely fixed in place by irradiation with a 100 W UV lamp. Then a 1 mm thick glass slide with a 1 cm diameter inset circular hole was placed on top of the electrodes and sealed to the electrodes with UV glue. Finally, immediately prior to use, the top of the chamber was closed by a 22 mm diameter, 170 μm thick circular coverslip. The use of optical quality coverslips on both the bottom and top of the sample chamber minimized spherical aberration.

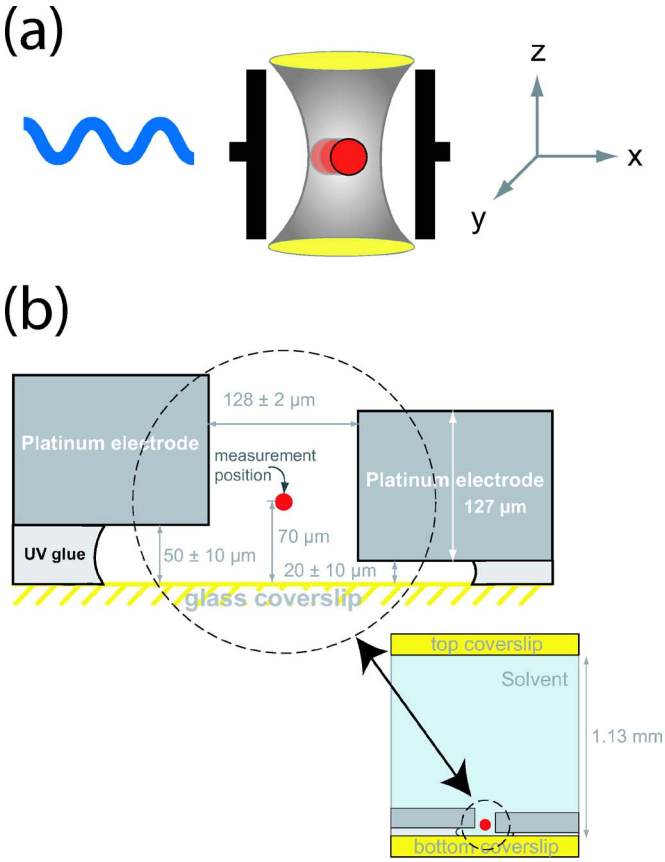

FIG. 2. (Color online) (a) Schematic of the optical microelectrophoresis experiment (not to scale). (b) Detailed geometry of the optical cell. The dispersion is sandwiched between two glass coverslips. The lower coverslip carries the two platinum electrodes.

The distance between the two electrodes was measured, after assembly of the cell, using a calibrated microscope graticule as 128±2 μm. The small gap between the electrodes made it possible to generate electric fields on the order of tens of kV/m with just a few volts applied to the cell. This low voltage operation minimizes thermal instabilities produced by Joule heating and guarantees the absence of electrohydrodynamic fluid instabilities, which have complicated earlier electrophoretic measurements at high voltages.[17] In a simple one-dimensional cell with two semi-infinite plane parallel electrodes, the electric field is simply $E=V/d$, where V is the applied voltage and d is the electrode spacing. In our experiments the electrode geometry is strictly two dimensional [Fig. 2(b)], which complicates an analysis of the electric field. Recognizing the similarity to the one-dimensional limit, it is convenient to express the electric field in the form $E=\lambda V/d$, where λ is a correction factor smaller than one that depends on the exact x and z positions. The electric field was calculated numerically for the geometry of Fig. 2(b) by finite element simulation (MAXWELL 2D, Ansoft Corporation, USA), taking the dielectric constants of the suspension and glass as 2 and 5.5, respectively. In Fig. 3 the normalized electric field λ is shown as a function of the elevation z in a plane halfway between the two electrodes. The results confirm that between the two electrodes the electric field is homogeneous, with the field changing by less than 5% in a 65 μm high zone in the middle of the electrodes. In all of the

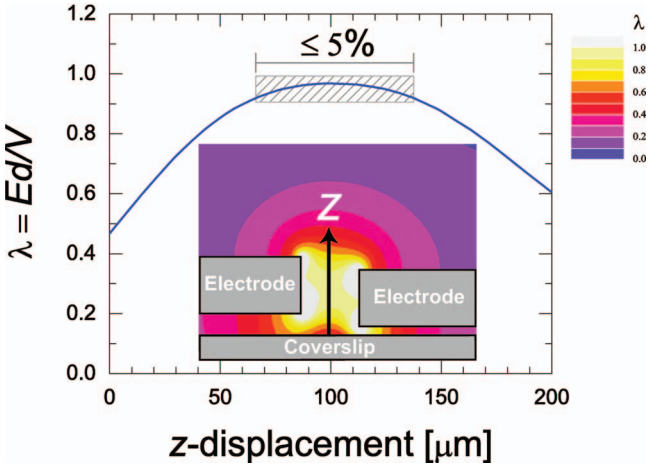

FIG. 3. (Color) Simulation of the electric field. The solid line shows the magnitude λ of the normalized electric field, midway between the two electrodes, as a function of the distance z from the lower coverslip. The field is approximately constant (within 5%) in the 65 μm wide hashed region between the two electrodes. The inset shows the simulated two-dimensional electric field contours in the vicinity of the electrodes.

experiments detailed below (unless otherwise stated) the particle was maintained in this zone of uniform E, at a typical elevation of $z=70$ μm. For the calculation of the particle charge we use the normalized field calculated at $x=0$ and $z=70$ μm of $\lambda=0.93$.

To prevent the development of nonuniform space charges near the electrodes, the electrophoretic motion was measured using an alternating electric field. Accumulation of ions at the electrode becomes important if the voltage is applied for a time of order of the transit time

$$\tau_{\mathrm{tr}} = \frac{d^2}{\mu_{\mathrm{cc}} V}, \tag{4}$$

where μ_{cc} is the mobility of the charge carriers. The characteristic time τ_{tr} is the time for charge carriers to move a distance of order of the electrode spacing d. In our experiments, where charge carriers are typically inverse micelles with a radius ≈ 2 nm, the transit time $\tau_{\mathrm{tr}}=\mathrm{O}(1)$ s. Consequently, provided that the frequency of the applied alternating field is large compared to τ_{tr}^{-1}, the concentration profile of ions between the electrodes will remain homogeneous and the electric field E unscreened. We used a minimum field frequency of $\omega_p=25$ rad s^{-1} to ensure that nonlinearity in the field is negligible.

Alternating electric fields have a further benefit in that they suppress undesirable electro-osmotic fluid flows.[18] The electric field simulations (Fig. 3) reveal that while the field on the top glass surface is essentially zero, the field E_t on the bottom glass wall remains finite ($\approx 50\%$ of the field between the electrodes). If the lower wall is charged, then an oscillatory fluid flow will develop at the base of the cell which could conceivably affect the motion of the optically trapped particle. In order to clarify the role of electro-osmosis we consider the time-dependent fluid flow produced by a single charged plane. Although detailed theoretical predictions are available for the electro-osmotic flow profiles generated at all distances from a wall,[19] we are interested primarily only in fluid flows at the particle location, far from the wall. Dutta and Beskok[20] showed that, in this limit, the electro-osmotic profile resembles the classical Stokes problem of a flat plate oscillating at a frequency ω_p in a semi-infinite fluid. In a fluid of viscosity η and dielectric constant ϵ the oscillatory flow $u(z,t)$ has the asymptotic form

$$u(z,t) = u_{\mathrm{HS}} \exp\left[-\frac{z}{\sqrt{2}l_D}\right] \sin\left[\omega_p t - \frac{z}{\sqrt{2}l_D}\right], \tag{5}$$

where $u_{\mathrm{HS}}=-\epsilon\zeta_w E_t/\eta$ is the steady-state Helmholtz-Smoluchowski electro-osmotic velocity, with E_t as the tangential electric field at the wall and ζ_w as the zeta potential of the wall. Equation (5) represents damped harmonic fluid oscillations. The oscillations decay on a characteristic length scale,

$$l_D = (\nu/\omega_p)^{1/2}, \tag{6}$$

where ν is the kinematic viscosity. An inspection of Eqs. (5) and (6) reveal that any artifacts due to electro-osmosis should be frequency dependent. At the highest frequencies used ($\omega_p \sim 1900$ rad s^{-1}) the characteristic length scale for momentum diffusion in the fluid ($l_D=31$ μm) is appreciably smaller than the separation between particle and wall ($z=70$ μm). Consequently, electro-osmosis should be unimportant. To confirm this we measured the field-induced motion of a single particle as the particle was moved towards the wall from $z=70$ μm to $z=30$ μm in 10 μm steps. The measured response was in excellent agreement with the calculated electric field profile shown in Fig. 3, confirming the absence of any significant electro-osmotic flows. The suppression of electro-osmosis was also supported by the observation, detailed in Sec. IV A, that measured mobilities were frequency independent. Any significant contribution of electro-osmosis to particle displacement would render the apparent mobilities frequency dependent. Consequently, for the typical experimental parameters used here electro-osmosis appears to be unimportant.

The sample chamber was filled with a dilute suspension of colloidal particles with a volume fraction of $\sim 10^{-5}$. The cell was carefully centered so that the laser passed through a plane equidistant between the two electrodes and the focus was midway between the top and bottom surfaces. The particle was held at least 65 μm from the nearest surface to ensure that Stokes' law was applicable. The charge on the particle was analyzed using a purposely written software package in interactive definition language (IDL, Research Systems, Boulder, Colorado). The sign was determined by reducing the frequency of the applied electric field to 0.5 Hz, blocking the laser beam so that the particle was momentarily released from the optical trap, and following the oscillatory motion of the free particle on a charge coupled device camera.

The accuracy of SPOM was checked by measuring the mobility of a 850 nm (radius) poly(methyl methacrylate) (PMMA) particle in dodecane [with 100 mM sodium bis(2-ethylhexyl) sulfosuccinate (NaAOT)] using a commercial PALS instrument (Brookhaven ZetaPlus), μ_{PALS}, and the SPOM technique, μ_{SPOM}. The good agreement between μ_{SPOM} $[(-5.6\pm0.5)\times10^{-10}$ m^2 s^{-1} V$^{-1}]$ and

μ_{PALS} $[(-6.0\pm0.5)\times10^{-10}$ m^2 s^{-1} V$^{-1}]$ confirms that the optical microelectrophoresis technique yields accurate particle mobility data.

III. THEORY

A colloidal particle illuminated by a laser beam encounters a gradient force that is oriented in the direction of the intensity gradient and a scattering force that is oriented in the direction of the incident light. In a tightly focused beam the gradient forces dominate and lead to a strong restoring force, which causes the particle to be confined near the focus of the beam. To a first approximation, the particle can be modeled as a mass m in a three-dimensional harmonic potential. The potential is characterized by two spring constants, one in the axial and one in the radial direction. Here, for simplicity, we analyze only the one-dimensional motion along the radial coordinate x, where the corresponding force constant is k_H.

Placed in an external electric field, the total force on a *charged* particle is a sum of three contributions: a harmonic force $-k_Hx(t)$ arising from the optical trap, a random force $\mathcal{R}(t)$ that represents thermal forces at the temperature T, and an external periodic force $F_p(t)=A\sin(\omega_pt+\phi)$, which is characterized by the frequency ω_p, amplitude A, and initial phase ϕ of the external field. Defining the *effective* electrokinetic charge on the particle as Z_{eff} (in units of the fundamental charge e), the amplitude of the oscillatory force may be written as

$$A = Z_{\mathrm{eff}}eE, \tag{7}$$

where E is the electric field strength at the particle. We assume below that the friction coefficient of a charged sphere of radius a is simply the classical Stokes result, $\xi=6\pi\eta a$, and ignore the small contribution to the friction from the flow-induced deformation of the ionic atmosphere around the particle. In consequence, Z_{eff} should be interpreted as a reparametrization of the electrophoretic mobility μ since balancing the electrical and frictional forces yields $Z_{\mathrm{eff}}=6\pi\eta a\mu/e$. In the Hückel limit, when $\kappa a\ll1$ and $e\zeta\lesssim k_BT$, the effective charge Z_{eff} is simply equal to the charge Z on the particle. Outside this limit no such equality holds.

In a single particle optical microelectrophoresis experiment, the quantity ultimately measured is the time-dependent particle autocorrelation function $C(\tau)$ or its Fourier transform, the spectral density $I(\Omega)$. Below, we derive expressions for both quantities in terms of the effective electrokinetic charge Z_{eff}.

A. A periodically driven Brownian oscillator

The fluctuations of a periodically driven Brownian oscillator are described in the conventional Ornstein-Uhlenbeck theory[21] by the Langevin equation

$$m\ddot{x}(t)+\xi\dot{x}(t)+k_Hx(t)=A\sin(\omega_pt+\phi)+\mathcal{R}(t). \tag{8}$$

Here, $x(t)$ is the particle trajectory. The random thermal forces are modeled by a Gaussian process $\mathcal{R}(t)$ with the moments

$$\langle\mathcal{R}(t)\rangle=0 \quad \text{and} \quad \langle\mathcal{R}(t)\mathcal{R}(t')\rangle=2\xi k_BT\delta(t-t'). \tag{9}$$

This definition ensures that the Brownian particle is in thermal equilibrium at a temperature T in the absence of any driving field, i.e., for $A=0$.

A colloidal particle, once moving, loses momentum rapidly as a result of viscous losses. The characteristic time for this decay is $t_B=m/\xi$, which is about 10^3 times smaller than the time resolution of our experiments, when digitizing at a 10 kHz sampling rate. Consequently, the inertial terms may safely be dropped so that Eq. (8) now reads

$$\xi\dot{x}(t)+k_Hx(t)=A\sin(\omega_pt+\phi)+\mathcal{R}(t). \tag{10}$$

The equation is linear so that the general solution may be written as[22]

$$x(t)=x_n(t)+x_p(t), \tag{11}$$

where x_n is the solution in the presence of random thermal forces *only* (i.e., $A=0$) and x_p is the solution when only periodic forces act (i.e., $T=0$). We now consider each solution in turn.

The driven oscillator is deterministic in the absence of any random thermal noise. The solution is well known,[22]

$$x_p(t)=\frac{A}{k_H[1+(\omega_p/\omega_c)^2]^{1/2}}\sin(\omega_pt+\phi-\Delta). \tag{12}$$

The particle motion lags the driving field by a constant phase factor,

$$\Delta=\tan^{-1}\frac{\omega_p}{\omega_c}, \tag{13}$$

which varies with the relative sizes of the driving and the *corner frequency*

$$\omega_c=k_H/\xi. \tag{14}$$

The frequency ratio ω_p/ω_c also controls the amplitude of the particle motion. For low frequencies ($\omega_p\ll\omega_c$) the amplitude is essentially frequency independent, while at high frequencies ($\omega_p\gg\omega_c$) the response decreases rapidly with increasing ω_p. In between, Eq. (12) reveals a monotonic oscillation spectrum, without the dynamic resonance at $\omega_p=\omega_c$, characteristic of underdamped systems. The relative phase of the particle motion depends on the initial phase ϕ of the applied force. In our experiments ϕ is a fluctuating stochastic variable with a coherence time τ_p, which depends on the stability of the voltage generator. The phase is essentially randomized on times $t\gg\tau_p$, so time and phase averages are equivalent. Multiplying the trajectories at t and t' and averaging over ϕ, assuming the initial value of ϕ is uniformly distributed over the interval $[0,2\pi]$, yields the correlation function,

$$\langle x_p(t)x_p(t')\rangle_\phi=\frac{A^2}{2k_H^2[1+(\omega_p/\omega_c)^2]}\cos\omega_p(t-t'), \tag{15}$$

where the subscript denotes the phase averaging. Since the motion is totally deterministic, $\langle x_p(t)x_p(t')\rangle_\phi$ oscillates continuously between positive and negative values.

The dynamics of the trapped particle is a linear superposition of periodic and random motions. The correlation function of a purely Brownian oscillator is given by Doi and Edwards[23] as

$$\langle x_n(\tau)x_n(0)\rangle_{\mathcal{R}} = \frac{k_BT}{k_H}\exp(-\omega_c\tau). \tag{16}$$

The mean-square displacement is accordingly $\langle x_n^2\rangle_{\mathcal{R}} = k_BT/k_H$ and, since $F=-k_Hx$, the mean-square thermal forces on the trapped particle are $\langle F_n^2\rangle_{\mathcal{R}} = k_BTk_H$.

B. Correlation function and spectral density

The correlation function $c(\tau)$ of the periodically driven Brownian oscillator is defined by

$$c(\tau = t' - t) = \langle\langle x(t)x(t')\rangle_{\mathcal{R}}\rangle_{\phi}, \tag{17}$$

where the averages are taken over both noise and phase. Since the thermal and periodic forces are uncorrelated, $c(\tau)$ is simply a sum of the correlation functions for periodic and purely thermal motions,

$$c(\tau) = \frac{k_BT}{k_H}\exp(-\omega_c\tau) + \frac{A^2}{2k_H^2[1+(\omega_p/\omega_c)^2]}\cos\omega_p\tau. \tag{18}$$

It is more convenient to work with the normalized function $C(\tau)=c(\tau)/c(0)$, which may be written as

$$C(\tau) = \frac{1}{1+\gamma^2}\exp(-\omega_c\tau) + \frac{\gamma^2}{1+\gamma^2}\cos\omega_p\tau, \tag{19}$$

where we have introduced γ^2, the scaled *ratio of the mean-square periodic and Brownian forces*,

$$\gamma^2 = \frac{\langle F_p^2\rangle/\langle F_n^2\rangle}{1+(\omega_p/\omega_c)^2}. \tag{20}$$

Here, $\langle F_p^2\rangle = Z_{\text{eff}}^2e^2E^2/2$ and $\langle F_n^2\rangle = k_BTk_H$. The force ratio γ appears naturally in the theory of a driven Brownian oscillator and, as we will show below, is also the quantity most readily extracted from experiment. Knowing γ, the charge on the particle follows immediately as

$$e|Z_{\text{eff}}| = \frac{\gamma\xi}{E}\sqrt{\frac{2k_BT}{k_H}(\omega_p^2+\omega_c^2)}. \tag{21}$$

This expression simplifies at low frequencies ($\omega_p \ll \omega_c$) to

$$e|Z_{\text{eff}}| = \frac{\gamma}{E}\sqrt{2k_BTk_H}, \tag{22}$$

which does not depend on the radius of the trapped particle.

Figure 4 shows the force ratio γ calculated for typical experimental parameters. In the weak-field limit where $\gamma \ll 1$, the motion of the trapped particle is dominated by random thermal forces. By contrast, in the strong-field limit where $\gamma \gg 1$, the thermal forces are only a relatively small perturbation and the electrophoretic forces dominate. The crossover between these two regimes occurs at a particle charge of $Z_{\text{eff}} \sim 20$ for typical field strengths. At this point the electric forces on the particle are a few hundred femtonewtons.

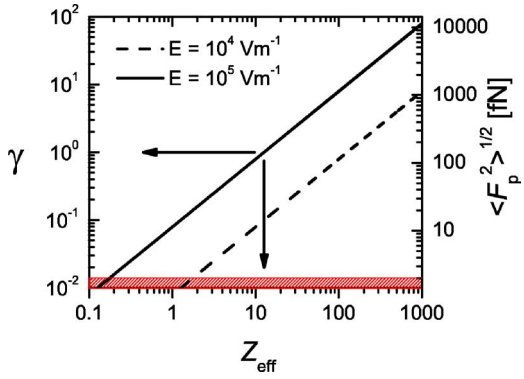

FIG. 4. (Color online) The dimensionless ratio γ of electric and Brownian forces. The trapped particle has a charge eZ_{eff} and is placed in an oscillatory electric field of amplitude E and frequency ω_p. The rms electrical forces (shown on the right-hand axis) are calculated, assuming $\omega_p \ll \omega_c$ and a force constant of $k_H=5$ fN nm^{-1}. The shaded region indicates the noise floor where the spectral density of the electric and Brownian forces are equal at ω_p. The boundary is calculated assuming $a=500$ nm, $\eta=1.38$ mPa s, and $t_0=26$ s. In the shaded region, the charge on the particle is too low to be detectable by the current technique. The limiting charge sensitivity is $\sim 2e$ and $0.2e$ for fields of 10^4 and 10^5 V m^{-1}, respectively.

The force ratio γ may be determined experimentally from the correlation function $C(\tau)$ or, equivalently, from the spectral density,

$$I(\Omega) = \frac{1}{2\pi}\int_{-\infty}^{\infty} c(\tau)\exp(-i\Omega\tau)d\tau. \tag{23}$$

As we will discuss below, there are advantages to both approaches. Inserting Eq. (18) into Eq. (23) reveals that the spectral density is a sum of two independent contributions,

$$I(\Omega) = \frac{k_BT}{\pi\xi}\frac{1}{\Omega^2+\omega_c^2} + \frac{k_BT\gamma^2}{2k_H}[\delta(\Omega-\omega_p)+\delta(\Omega+\omega_p)], \tag{24}$$

a Lorentzian spectrum typical of the Brownian motion in a harmonic potential, together with additional δ spikes at the positive and negative field frequencies. Integrating the spikes over the frequency axis gives an expression for the mean-square periodic displacement of the particle

$$P_{\text{sig}} = \int_{-\infty}^{\infty} I_p(\Omega)d\Omega = \frac{k_BT}{k_H}\gamma^2, \tag{25}$$

from which γ can be found.

C. Asymptotic probability distribution function

We now turn to the probability distribution of the confined particle. Introducing the dimensionless position coordinate $\bar{x}=x/(k_BT/k_H)^{1/2}$, we define the probability of locating the Brownian particle in the region between $\bar{x}$ and $\bar{x}+d\bar{x}$ as $p(\bar{x})d\bar{x}$, where $p(\bar{x})$ is the probability distribution function.

Without a periodic force, the Brownian particle is at thermal equilibrium and $\bar{x}(t)$ follows the Boltzmann distribution,

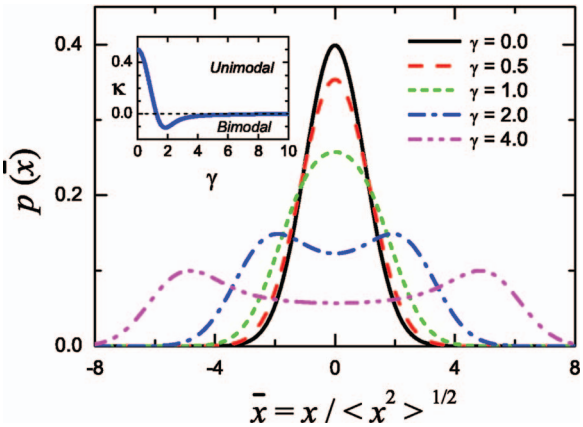

FIG. 5. (Color) The balance between thermal and electric forces. The full lines show the dependence of the asymptotic probability distribution $p(\bar{x})$ on the ratio γ of the electric and thermal forces. The inset plot shows the curvature κ of $p(\bar{x})$, evaluated at the origin $\bar{x}=0$. The probability distribution is double peaked for $\gamma \geqslant 1.257$ where κ changes sign.

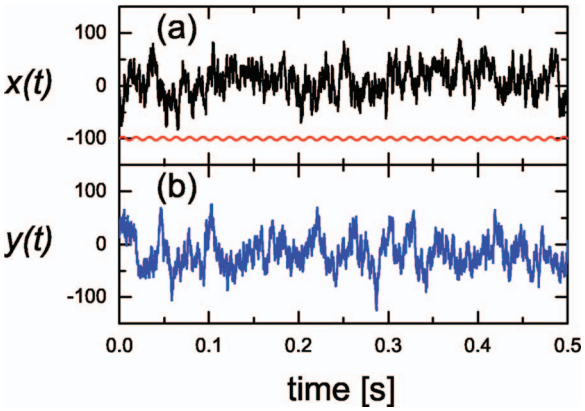

FIG. 6. (Color) Time trace of the x and y coordinates of a charged particle in a sinusoidal electric field. The field was aligned along the x axis and had a frequency of 67 Hz and an amplitude of 13.3 kV m^{-1}. Periodic oscillations are not visible in the measured trajectory, which is dominated by random Brownian fluctuations. The relative size of the periodic oscillations expected are illustrated by the lower curve in (a).

$$p_n(\bar{x}) = \frac{1}{\sqrt{2\pi}} \exp(-\bar{x}^2/2). \tag{26}$$

Applying a time-dependent force perturbs the system and shifts the average distribution away from the equilibrium result. When all transients have died out, the probability approaches a new asymptotic distribution which is a periodic function of the time t. As discussed earlier, the only experimentally accessible quantities are the phase-averaged functions. Analytical expressions for the phase-averaged distributions have been proposed by Jung and Hänggi[24] for arbitrary friction coefficients. In the overdamped limit, their result reduces to the infinite series

$$p(\bar{x}) = \frac{1}{\sqrt{2\pi}} \exp\left(-\frac{\bar{x}^2+\gamma^2}{2}\right)\left\{ I_0\left(\frac{\gamma^2}{2}\right) I_0(\sqrt{2}\gamma\bar{x}) + 2\sum_{k=1}^{\infty} (-1)^k I_k\left(\frac{\gamma^2}{2}\right) I_{2k}(\sqrt{2}\gamma\bar{x}) \right\}, \tag{27}$$

where $I_k(x)$ is a modified Bessel function.[25] Figure 5 shows the effect of a finite external field on the probability distribution. With increasing amplitude, the probability $p(\bar{x})$ first broadens until, at $\gamma=\gamma^*$, the distribution becomes bimodal and develops two peaks around $\bar{x} \sim \pm\gamma$. Further increases in the external field cause the two peaks to split further apart, leaving a relatively flat distribution around the origin, as the particle becomes increasingly localized around the two extremities.

The changes in the probability distribution with external field can be clearly seen from the curvature of $p(\bar{x})$ near the origin. Expanding Eq. (27) around $\bar{x}=0$ gives, to terms in $\bar{x}^2$,

$$p(\bar{x}) = \frac{1}{\sqrt{2\pi}} \exp\left(-\frac{\gamma^2}{2}\right) I_0\left(\frac{\gamma^2}{2}\right)(1-\kappa\bar{x}^2), \tag{28}$$

where the curvature is

$$\kappa = \frac{1}{2}\left[1 - \gamma^2 + \gamma^2 \frac{I_1(\gamma^2/2)}{I_0(\gamma^2/2)}\right]. \tag{29}$$

κ is positive for a single monomodal distribution and negative for a bimodal distribution. The inset plot in Fig. 5 displays the variation of κ with external field. The curvature first decreases rapidly with increasing γ, reflecting the broadening of $p(\bar{x})$ evident at low modulation strengths, before changing sign for $\gamma > \gamma^* = 1.257$ as the distribution becomes bimodal. The small negative values of the curvature found at high fields correspond to the extremely flat shape of the distribution seen close to the origin at high γ. The curvature is a function solely of γ^2 so that the distribution sharpens continuously with increasing frequency and does not show the resonant bimodality evident in the underdamped limit.[24]

The width of the particle distribution is $\langle x^2 \rangle$, which is from Eq. (18),

$$\langle x^2 \rangle = \frac{k_B T}{k_H}(1+\gamma^2), \tag{30}$$

where $\langle \cdots \rangle$ denotes an average over both $\mathcal{R}$ and ϕ. In the weak-field limit where $\gamma \ll 1$, the width of the distribution approaches the thermal limit, $k_B T/k_H$. Broadening of the probability distribution is only significant in the strong-field limit ($\gamma \gg 1$) where the width varies quadratically with the strength of the applied field.

IV. RESULTS AND DISCUSSION

A. Field and frequency dependence of effective charge

To validate our technique, experiments were first carried out on a number of weakly charged particles as a function of the applied field strength and its frequency. The particles were taken from a dilute dispersion of 610 nm (radius) poly-(methyl methacrylate) particles in a 0.035 wt % solution of a PHSA-g-PMMA copolymer ($\kappa a = 0.65$) in dodecane. Figure 6 shows a short portion of the x and y positions of a trapped particle when a sinusoidal field is applied. The field was

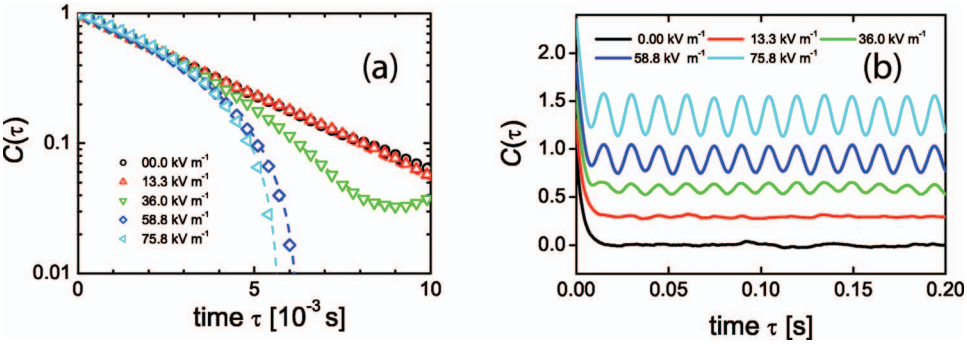

FIG. 7. (Color) The measured autocorrelation function $C(\tau)$. The sample was a PMMA particle in dodecane (containing 0.035 wt % free PHSA-*g*-PMMA copolymer). Data were recorded for 26 s at each field. The driving frequency ω_p was 420.8 rad s^{-1}. (a) shows that at short delay times the measured autocorrelations collapse to a single exponential decay. The dashed lines in (a) are least-squares fits to Eq. (19), with a corner frequency of 295±7 rad s^{-1}. (b) reveals the periodic correlations found at long delay times. The curves have been vertically displaced for clarity.

applied along the x axis, so periodic oscillations are expected in the x signal and should be absent from the y signal. Looking at the trajectories plotted in Fig. 6, it is very difficult to see any significant differences between the x and y signals. The small electrophoretic oscillations expected are "buried" beneath much larger Brownian fluctuations and $\gamma \ll 1$. To extract the small periodic excursions from the predominantly random Brownian motion, we determine the spectral distribution of the fluctuations.

Figure 7 shows the normalized autocorrelation functions, $C(\tau)$, measured on the same particle, as the applied field was varied. The oscillatory component is clearly visible, particularly at long times. Data collection is fast with each of the functions shown representing just 26 s worth of data. The alternating electric field had a frequency of 67 Hz, and voltages of up to 10 V were applied to the electrodes. The laser trap had a stiffness of $k_H = 4.7 \pm 0.1$ fN nm^{-1} and a corner frequency of 47±1 Hz. The agreement between the experimental data and the least-squares fits is excellent. Figure 7(a) reveals that at short times the correlation functions all essentially converge, even though their long time dependence is clearly very different. This is because on time scales shorter then the period of the applied field, the motion of the trapped particle is dominated by the Brownian diffusion. Thermal fluctuations are independent of the field and, since they are uncorrelated, result in the exponential relaxation apparent at short times in $C(\tau)$ [Eq. (16)]. The oscillations evident at long times [Fig. 7(b)] reflect the periodic motion produced by the applied field and accordingly grow as the applied field is increased.

Fitting the measured correlation functions to the theoretical expression for $C(\tau)$ [Eq. (19)] yields γ, the ratio of the rms electrophoretic and Brownian forces. The ratio is plotted in Fig. 8 as a function of the applied field E. As expected, the experimental values of γ are linearly proportional to E, confirming that the charge on the particle is constant. The gradient of the plot yields an effective charge of $|Z_{\text{eff}}| = 14.5e \pm 0.2e$, equivalent to an electrophoretic mobility of $\mu = (1.46 \pm 0.02) \times 10^{-10}$ m^2 s^{-1} V^{-1}. The charge on this particle is sufficiently low that, even at the maximum field strengths achievable, the system remains in the low-field limit ($\gamma < 1$) where Brownian forces dominate.

For ultralow charges where $\gamma \ll 1$ it becomes increasingly difficult to determine the oscillatory element in the autocorrelation function because of fluctuations in the base line. This can be seen in the data at 13.3 kV m^{-1} in Fig. 7(b), where the oscillations are indistinct. To resolve these low particle charges we perform a fast Fourier transform of the data and calculate the spectral density. Figure 9 shows the field dependence of the resulting power spectra. The measured spectra are particularly simple, being a superposition

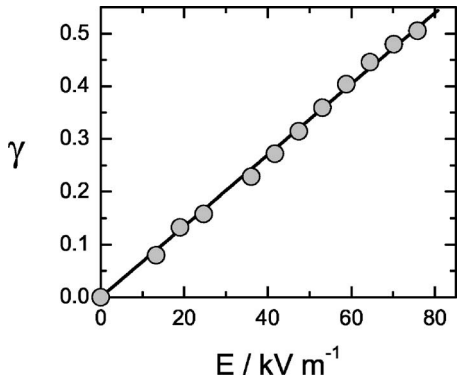

FIG. 8. The field dependence of the force ratio γ. γ was obtained by fitting the autocorrelations displayed in Fig. 7 to Eq. (19). The linear variation of γ with the field E confirms that the charge on the particle is independent of the strength of the applied field. The solid line yields an effective charge of $|Z_{\text{eff}}| = 14.5 \pm 0.2$.

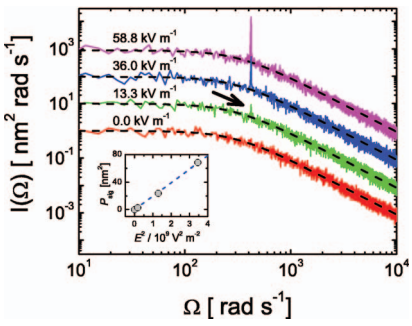

FIG. 9. (Color) The field dependence of the spectral density $I(\Omega)$. The sample was a 610 nm PMMA particle suspended in dodecane with 0.035 wt % added PHSA-*g*-PMMA copolymer. The variance of the power spectrum was reduced by averaging together 64 spectra, calculated from consecutive trajectories each containing 2^{14} data points ($t_0 = 1.64$ s) recorded on the same particle.

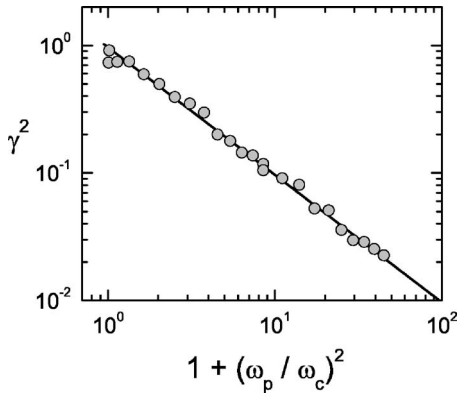

FIG. 10. The frequency dependence of the force ratio γ. The amplitude of the electric field was fixed at $E=75.8$ kV m^{-1} and the frequency ω_p varied. The solid line is a least-squares fit of log γ^2 against $\log(1+(\omega_p\,\omega_c)^2)$ with a gradient of -0.98 ± 0.02.

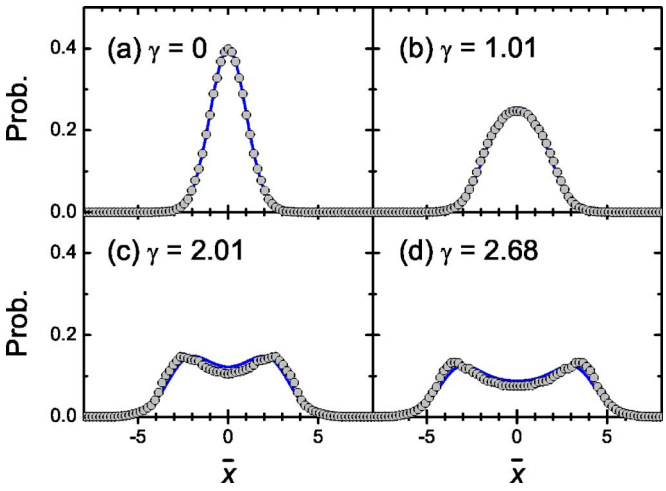

FIG. 11. (Color online) The probability distributions characterizing the restricted diffusion of an optically trapped PMMA particle in a solution of 100 mM Na-AOT in dodecane. The corner frequency of the optical trap was 25.0 Hz. The points give the measured distribution in electric fields of amplitudes (a) 0 kV m^{-1}, (b) 22.8 kV m^{-1}, (c) 45.5 kV m^{-1}, and (d) 60.7 kV m^{-1}. The sinusoidal electric field had a frequency of 17.5 Hz. The solid lines were calculated from the theory for a driven harmonically bound particle [Eq. (27)] using experimentally measured parameters. The comparison has no adjustable parameters.

of a Lorentzian spectrum (shown dashed) reflecting diffusive motion and a single δ peak at the fundamental electrode drive frequency ω_p, whose height increases with the applied field. The data contain no higher harmonics of ω_p, confirming the linear response of particle and field. To extract the power in the periodic signal, the data around the δ spike were masked and the diffusive spectrum fitted to the first term of Eq. (24) by adjusting the unknown corner frequency ω_c. Subtracting the fitted Lorentzian from the measured power spectra yielded the signal spectrum. The mean-square electrophoretic displacement P_{sig} was obtained by integrating the signal spectrum around the peak at ω_p. The resulting values for P_{sig} are plotted as a function of the square of the applied field, in the inset in Fig. 9. As expected from Eq. (25), the mean-square displacement P_{sig} varies linearly with E^2. The high positional sensitivity achievable is highlighted by the arrowed δ peak in Fig. 9 which, while it remains clearly visible, corresponds to a mean-square displacement of only 1.4 nm^2.

To explore how the frequency of the applied field influenced the measurements, we collected autocorrelations at a number of different field frequencies, taking care to ensure that the same particle was used in each case. The corner frequency of the trapped particle was $\omega_c=291$ rad s^{-1}, and data were recorded at frequencies between 25 and 1930 rad s^{-1}, approximately an order of magnitude below and above the corner frequency of the optical trap. The amplitude of the applied field was fixed at 75.8 kV m^{-1}. The autocorrelations were analyzed as described above to determine γ^2 at each frequency. The results are summarized in Fig. 10. As expected, from the discussion in Sec. III A, the response of the trapped particle to the applied field decreases with increasing frequency. This drop in sensitivity is particularly sharp when the driving frequency exceeds the corner frequency of the optical trap. Plotting γ^2 as a function of the frequency ratio $1+(\omega_p/\omega_c)^2$ confirms that γ^2 is inversely dependent on $1+(\omega_p/\omega_c)^2$, in agreement with the predictions of Eq. (20). The highly linear dependency evident in Fig. 10 confirms the validity of the driven harmonic model and indicates that the electrophoretic mobility of the particle is essentially frequency independent, at least in the relatively narrow band of frequencies between 4 and 300 Hz. An analysis gives the surface charge on the particle as $|Z_{\mathrm{eff}}|=15.8\pm0.2$. Although dynamic electrophoretic mobility has been intensely studied theoretically, there have been been relatively few experimental studies to date.[26] Two possible relaxation processes have been proposed[27] for an isolated colloidal particle with characteristic times that are determined by ion diffusion either on scales of the particle radius a or the Debye length κ^{-1}. In our samples, the characteristic times of both processes are estimated to be about 10^{-3} s, so relaxation processes are expected at higher frequencies than those studied here. Further experiments with a wider range of frequencies are planned to explore the full relaxation behavior of the mobility.

B. Field dependence of probability distribution function

So far, we have found an excellent agreement between our measurements and the theoretical predictions for a periodically driven oscillator. The comparison, however, has been limited to weakly charged particles where $\gamma<1$. To extend our understanding, we now look at more highly charged particles where strong electrophoretic forces dominate the weaker Brownian forces. Hsu *et al.* has shown[3] that nonpolar suspensions may be charged by adding the surfactant, Na-AOT, which forms reverse micelles in a nonpolar solvent. Adding Na-AOT to our suspensions at concentrations of 100 mM increases the average charge (in electrons) on the PMMA particles by a factor of 4 to $Z_{\mathrm{eff}}\approx-50$. Using these more highly charged particles, we are able to investigate the high-field limit where $\gamma>1$.

Figure 11 shows the field dependence of the particle probability. The normalized distribution function is plotted as a function of the dimensionless position $\bar{x}=x/(k_BT/k_H)^{1/2}$,

where the x location of the sphere has been scaled by the size of the corresponding rms Brownian fluctuations in the optical trap. To correct for small asymmetries in the trap caused by optical misalignment, the measured probability was averaged together at each positive and negative displacement. The resulting symmetrized distributions, $p_s(\bar{x})=[p(\bar{x})+p(-\bar{x})]/2$, are plotted in Fig. 11. At zero field the probability distribution is a simple Gaussian function, as expected from Eq. (26). Increasing the field to $E\approx 23$ kV m^{-1} causes the distribution to broaden, although it remains singly peaked. At fields of 46 kV m^{-1} and above there is a dramatic change in $p_s(\bar{x})$. The central peak in the distribution first splits into two broad maxima, before then moving further apart in $\bar{x}$ as the field is increased still further. Using the experimentally determined charge on the particle ($Z_{\mathrm{eff}}=-48.3\pm0.3$) and the measured optical trap stiffness, we calculate the force ratio γ from the applied electric field E. In this way we have confirmed that the probability distribution first becomes bimodal at a force ratio in the range $1.01<\gamma<1.34$. This observation is in good agreement with the theoretical predictions of Sec. III C, where a bimodal distribution is predicted for $\gamma>\gamma^{*}=1.257$.

To account for the dramatic changes evident in the measured distributions, we have calculated $p(\bar{x})$ for a periodically driven oscillator. The exact shape of this distribution depends solely on the force ratio γ, as noted in Sec. III C. Fixing γ at the experimental value, we have evaluated numerically the series of Bessel functions given in Eq. (28). The infinite series was truncated when convergence to four significant figures was achieved. The results of these calculations are plotted as the solid lines in Fig. 11. The agreement is remarkably good and is particularly encouraging, given that there are no adjustable parameters in the comparison.

C. Sensitivity limit

The smallest charge that can be detected by our technique is fixed by the point where the peak in the spectral density at ω_p (the arrowed peak in Fig. 9) becomes indistinguishable from the Brownian background. At this point the spectral power in a band of width $\Delta\omega$ centered on ω_p is $P_{\mathrm{sig}}=\Delta\omega\cdot(k_BT/\pi\xi)/(\omega_c^2+\omega_p^2)$. The corresponding ratio of electric to Brownian forces is $\gamma^2=\Delta\omega\cdot\omega_c/\pi(\omega_c^2+\omega_p^2)$ and the smallest detectable particle charge is therefore

$$e|Z_{\mathrm{eff}}^{\mathrm{min}}|=\frac{\sqrt{12k_BT\eta a\Delta\omega}}{E}, \tag{31}$$

where we have used Eq. (25). In a discrete Fourier transform the minimum width $\Delta\omega$ of a frequency channel is determined by the total time t_0 of data acquisition and equals $\Delta\omega=2\pi/t_0$. In our system where $a=610$ nm, $\eta=1.38$ mPa s, and the maximum field strength is $E\sim 80$ kV m^{-1}, the minimum detectable charge is about $0.25e$ for an experimental run of $t_0=26$ s. This is equivalent to a limiting electrophoretic mobility of $\sim 2.5\times10^{-12}$ m^2 V^{-1} s^{-1}.

D. Measurement of charge distributions

We have shown that optical microelectrophoresis provides an accurate, rapid, and highly sensitive determination of the effective charge on an individual trapped particle. In many cases, of course, the population from which the single particle is selected is heterogeneous. There is a distribution of particle charges which reflects, for instance, the stochastic nature of the charging mechanism or variations in the surface chemistry or the size of individual particles. Many of the conventional methods used to probe the electrokinetics of colloidal suspensions (microelectrophoresis, laser Doppler electrophoresis, and electroacoustics) only allow for the calculation of the average mobility. They provide either little or no information on the distribution of particle charges. In many cases, however, knowledge of the charge distribution is of vital importance. Colloidal suspensions have, for example, proven to be valuable model systems in condensed matter physics. There is strong evidence that the width of the charge distribution (the charge polydispersity) significantly influences the glass transition and at high levels may suppress the freezing transition in these systems.[28] It is therefore important that techniques which allow an accurate characterization of the charge distribution are available.

We consider a suspension of colloidal particles with (effective) charges Ze which are distributed according to a normalized charge distribution function $P(Z)$. The mean charge and charge polydispersity σ_Z are defined by

$$\bar{Z}=\int_0^\infty P(Z)ZdZ, \tag{32}$$

$$\sigma_Z=\frac{1}{|\bar{Z}|}\left(\int_0^\infty P(Z)(Z-\bar{Z})^2\right)^{1/2}. \tag{33}$$

To characterize the charge distribution we trap and measure the effective charge of 50–100 individual particles. Although a little tedious, these repeated measurements are still quick. For instance, it takes a couple of minutes per particle to manually measure its charge: 20–30 s scanning time to locate a particle, a short delay of 30 s to center the particle trap, and a further 30 s for data collection.

To explore the range of applicability and resolution of the technique, we determined the charge distribution in nonpolar suspensions of PHSA-coated PMMA spheres. These colloidal spheres have been widely used in fundamental studies of nucleation, crystallization, and glass formation since the coating with PHSA is thought to provide a hard-sphere-type interaction. Figure 12(a) shows the charge distribution measured for PHSA-coated PMMA spheres suspended in clean dry dodecane. Clearly, the particles are very weakly charged, with an average colloidal charge of just three electrons per sphere, equivalent to an electrophoretic mobility of $\mu=-3\times10^{-11}$ m^2 s^{-1} V^{-1} and a zeta potential of -3.5 mV. Indeed, the particle mobility was sufficiently small to be undetectable on a commercial PALS instrument. The low mobilities, however, presented no problems for the optical microelectrophoresis measurements, as the data in Fig. 12(a) confirm. Although the charge on the PHSA-coated spheres is small, it is clearly nonzero, and so we expect a weak, soft repulsion between the particles. To gauge the level of this repulsion we estimate the average contact value U_0 of the interaction potential between spheres. An average charge

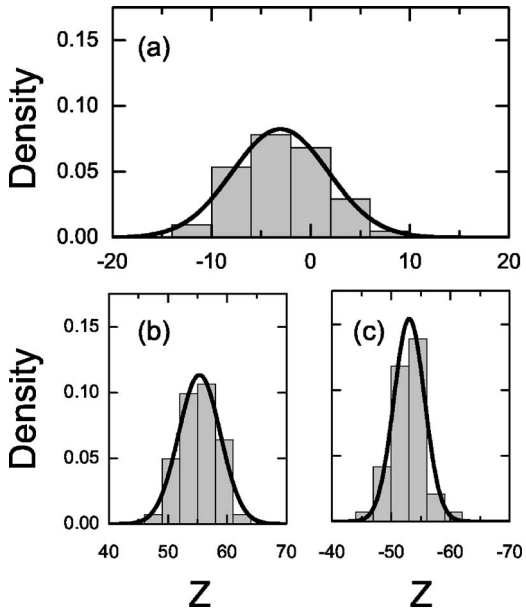

FIG. 12. The charge probability distribution measured for PMMA particles in dry dodecane with (a) no added surfactant, (b) 2 mM zirconyl 2-ethyl hexanoate (κa=0.55), and (c) 2 mM sodium-AOT (κa=0.30). The full lines are Gaussian fits.

of $\bar{Z}$=−2.9 equates to a value of U_0/k_BT=0.2 in dodecane [Eq. (1)]. Although the value is small in comparison to thermal energies, it cannot be ignored in quantitative studies. This is highlighted by, for instance, the recent studies of Auer *et al.*[29] who have explored the effect of a very similarly sized weak repulsion on the crystallization rate. They found that soft spheres crystallize some two orders of magnitude faster than a comparable system of pure hard spheres. Clearly, for quantitative studies, it is important to fully characterize the interaction potential, and optical microelectrophoresis offers a promising alternative to existing techniques.

The data in Fig. 12(a) reveal a second distinctive feature. The suspension is amphoteric in that it contains both positively and negatively charged spheres. Close to two-thirds of the particles are negative and the remainder are positive. While the charge distribution seems to be approximately Gaussian in shape, the width is broad with a charge polydispersity of σ_Z=1.5±0.3, which is surprisingly large. A more detailed discussion on the mechanism of charging will be given elsewhere.

As a further example of the applicability of the optical electrophoresis method, Figs. 12(b) and 12(c) show the effect of adding the surfactants $Zr(Oct)_2$ and Na-AOT, respectively, at concentrations of 2 mM to dilute PMMA suspensions in dodecane. These surfactants form reverse micelles in nonpolar solvents such as dodecane. A finite fraction of these micelles spontaneously ionize at room temperature.[30] Particles then acquire charge either by preferentially adsorbing the micelles of one sign or by dissociating a surface group, with the subsequent ionic species being solubilized within a reverse micelle. While the micelle-mediated charging of colloids has been known for at least the last 60 years,[4] the exact mechanism of charging in nonpolar media remains problematic and is not well understood. Figure 12 reveals that the addition of $Zr(Oct)_2$ causes the PMMA spheres to become strongly positively charged, while Na-AOT generates a large negative particle charge. Using the Hückel equation,[5] we calculate the equivalent zeta potentials to be +63 mV for the $Zr(Oct)_2$ treated spheres and −60 mV for the AOT containing suspensions. A comparable value for the zeta potential of around −38 mV was found by Kitahara *et al.*[31] for PMMA particles in cyclohexane with added AOT, while Hsu *et al.*[3] observed significantly higher zeta potentials of around −140 mV for PMMA in dodecane. In the case of $Zr(Oct)_2$, data are more limited, although Croucher *et al.*[32] reports that poly(vinyl acetate) particles are charged positive by the zirconyl salt. Surprisingly, we find that the charge distribution of the zirconyl and AOT suspensions are very sharply peaked with charge polydispersities of 5.0%±0.5% for the AOT system and 5.8%±0.6% for $OEHZr(Oct)_2$. In both cases the charge polydispersities are comparable, allowing for the sampling errors, to the size polydispersity of the colloid (4.6%±1%).

Finally, we point out that the majority of measurements of electrophoretic mobilities made to date have mainly been performed on suspensions with a low but finite particle concentration. Measurements on isolated or even very dilute systems of colloidal spheres are generally very rare.[13,33] Of particular interest in this context is the recent study[33] of the mobility of isolated highly charged latex spheres in a low-salt regime in water. The authors report strong and to date unresolved deviations from the mobility values expected for the Hückel limit, with the observation of extremely low mobilities at high dilution. These observations are particularly intriguing since the mobility of isolated spherical colloids has been intensively studied theoretically. The nonpolar systems and single particle technique detailed here offer the possibility of studying the electrokinetics of isolated hard spheres and carefully testing the intriguing observations of Ref. 33 in a very different chemical system. Detailed information on the electrophoretic mobility of a model system of isolated charged hard spheres will be published elsewhere.

V. CONCLUSIONS

In summary, we have demonstrated an ultrasensitive technique for the direct measurement of colloidal charges in nonpolar suspensions. The charge is measured by confining an individual particle to a harmonic optical potential and by following the excitation of the particle by a sinusoidal electric field. The trapped particle forms a strongly damped oscillator. By using a weak optical trap and an interferometric position detector, we have shown that single particle optical microelectrophoresis (SPOM) is capable of very high sensitivity. Surface charges on the level of a few elementary charges can be detected on individual colloidal particles, with an uncertainty of about 0.25*e*. Other techniques of measuring the charge on a particle are generally less sensitive. Our measurements are rapid and reproducible, with data on a single particle being recorded in approximately 30 s. When applied to multiple particles, our technique yields information on the distribution of particle charges rather than simply records the average charge, as provided by most conven-

tional electrokinetic techniques. These characteristics make SPOM ideal for the characterization of nonpolar suspensions and may prove useful in the study of fundamental phenomena in colloid chemistry, such as the relaxation of the double layer. For example, one might be able to detect discrete changes in the charge on a particle due to the time-dependent relaxation of the double layer. Work exploring these possibilities is currently underway.

ACKNOWLEDGMENTS

The authors wish to thank Unilever for partial funding and for permission to publish these results. Support from the UK Engineering and Physical Sciences Research Council is gratefully acknowledged. Adele Donovan is thanked for her help with particle synthesis and Kirsty Paul for PALS measurements.

[1] R. E. Kornbrekke, I. D. Morrison, and T. Oja, Langmuir **8**, 1211 (1992).
[2] W. H. Briscoe and R. G. Horn, Langmuir **18**, 3945 (2002); R. I. Keir, Suparno, and J. C. Thomas, *ibid.* **18**, 1463 (2002); J. C. Thomas, B. J. Crosby, R. I. Keir, and K. L. Hanton, *ibid.* **18**, 4243 (2002); C. E. McNamee, Y. Tsujii, and M. Matsumoto, *ibid.* **20**, 1791 (2004); P. G. Smith, W. Ryoo, and K. P. Johnston, J. Phys. Chem. B **109**, 20155 (2005).
[3] M. F. Hsu, E. R. Dufresne, and D. A. Weitz, Langmuir **21**, 4881 (2005).
[4] I. D. Morrison, Colloids Surf., A **71**, 1 (1993).
[5] R. J. Hunter, *Zeta Potential in Colloid Science: Principles and Applications* (Academic, London, 1981).
[6] R. W. O'Brien and L. R. White, J. Chem. Soc., Faraday Trans. 2 **74**, 1607 (1978).
[7] F. Carrique, F. J. Arroyo, and A. V. Delgado, J. Colloid Interface Sci. **252**, 126 (2002).
[8] P. Royall, M. E. Leunissen, and A. van Blaaderen, J. Phys.: Condens. Matter **15**, S3581 (2003); M. E. Leunissen, C. G. Christova, A.-P. Hynninen, C. P. Royall, A. I. Campbell, A. Imhof, M. Dijkstra, R. v. Roij, and A. van Blaaderen, Nature (London) **437**, 235 (2005); P. Bartlett and A. I. Campbell, Phys. Rev. Lett. **95**, 128302 (2005).
[9] B. Comiskey, J. D. Albert, H. Yoshizawa, and J. Jacobson, Nature (London) **394**, 253 (1998); Y. Chen, J. Au, P. Kazlas, A. Ritenour, H. Gates, and M. McCreary, *ibid.* **423**, 136 (2003); S. A. Jones, G. P. Martin, and M. B. Brown, J. Pharm. Sci. **95**, 1060 (2006).
[10] K. Schatzel and J. Merz, J. Chem. Phys. **81**, 2482 (1984); J. F. Miller, K. Schatzel, and B. Vincent, J. Colloid Interface Sci. **143**, 532 (1991).
[11] A. T. Perez and E. Lemaire, J. Colloid Interface Sci. **279**, 259 (2004).
[12] F. Strubbe, F. Beunis, and K. Neyts, J. Colloid Interface Sci. **301**, 302 (2006).
[13] N. Garbow, M. Evers, and T. Palberg, Colloids Surf., A **195**, 227 (2001).
[14] R. Galneder, V. Kahl, A. Arbuzova, M. Rebecchi, J. O. Rädler, and S. McLaughlin, Biophys. J. **80**, 2298 (2001).
[15] L. Antl, J. W. Goodwin, R. D. Hill, R. H. Ottewill, S. M. Owens, S. Papworth, and J. A. Waters, Colloids Surf. **17**, 67 (1986).
[16] F. Gittes and C. F. Schmidt, Opt. Lett. **23**, 7 (1998).
[17] V. J. Novotny, in *Colloids and Surfaces in Reprographic Technology*, ACS Symposium Series Vol. 200, edited by M. L. Hair and M. D. Croucher (American Chemical Society, Washington DC, 1982), pp. 281–306.
[18] M. Minor, A. J. van der Linde, H. P. van Leeuwen, and J. Lyklema, J. Colloid Interface Sci. **189**, 370 (1997).
[19] O. Soderman and B. Jonsson, J. Chem. Phys. **105**, 10300 (1996).
[20] P. Dutta and A. Beskok, Anal. Chem. **73**, 5097 (2001).
[21] G. E. Uhlenbeck and L. S. Ornstein, Phys. Rev. **36**, 823 (1930).
[22] M. L. Boas, *Mathematical Methods in the Physical Sciences*, 3rd ed. (Wiley, New York, 2006).
[23] M. Doi and S. F. Edwards, *The Theory of Polymer Dynamics*, 1st ed. (Oxford University Press, New York, 1988).
[24] P. Jung and P. Hanggi, Phys. Rev. A **41**, 2977 (1989).
[25] M. Abramowitz and I. A. Stegun, *Handbook of Mathematical Functions* 9th ed. (Dover, New York, 1972), p. 374.
[26] D. Mizuno, Y. Kimura, and R. Hayakawa, Langmuir **16**, 9547 (2000); Phys. Rev. Lett. **87**, 088104 (2001); Phys. Rev. E **70**, 011509 (2004).
[27] R. W. O'Brien, J. Fluid Mech. **190**, 71 (1988).
[28] B. V. R. Tata and A. K. Arora, J. Phys.: Condens. Matter **7**, 3817 (1995).
[29] S. Auer, W. C. K. Poon, and D. Frenkel, Phys. Rev. E **67**, 039904 (2003).
[30] H. F. Eicke, M. Borkovec, and B. Das-Gupta, J. Phys. Chem. **93**, 314 (1989).
[31] A. Kitahara, T. Satoh, S. Kawasaki, and K. Kon-No, J. Colloid Interface Sci. **86**, 105 (1982).
[32] M. D. Croucher, K. P. Lok, R. W. Wong, S. Drappel, J. M. Duff, A. L. Pundsack, and M. L. Hair, J. Appl. Polym. Sci. **30**, 593 (1985).
[33] N. Garbow, M. Evers, T. Palberg, and T. Okubo, J. Phys.: Condens. Matter **16**, 3835 (2004).